LAWRENCE
LIVERMORE
NATIONAL
LABORATORY

LLNL-JRNL-424563

TEMPEST Simulations of the Plasma Transport in a Single-Null Tokamak Geometry

X.Q. Xu, K. Bodi, R.H. Cohen, S. Krasheninnikov, T.D. Rognlien

February 24, 2010

Nuclear Fusion

Disclaimer

TEMPEST simulations of the plasma transport in a single-null tokamak geometry[1]

X. Q. Xu[1], K. Bodi[2], R. H. Cohen[1], S. Krasheninnikov[2], T. D. Rognlien[1],

[1)] Lawrence Livermore National Laboratory, Livermore, CA 94550 USA

[2)] University of California, San Diego, La Jolla, CA 92093 USA

e-mail contact of main author: xxu@llnl.gov

Abstract. We present edge kinetic ion transport simulations of tokamak plasmas in divertor geometry using the fully nonlinear (full-f) continuum code TEMPEST. Beside neoclasiocal transport, a term for divergence of anomalous radial flux is added to mock up the effect of turbulent transport. TEMPEST simulations were carried out for plasma transport and flow dynamics in a single-null tokamak geometry, including the pedestal region that can extend across the separatrix into the scrape-off layer (SOL) and private flux region. A series of TEMPEST simulations were conducted to investigate the transition of midplane pedestal heat flux and flow from the neoclassical to turbulent limit and the transition of divertor heat flux and flow from the kinetic to the fluid regime via an anomalous transport scan and a density-scan. The TEMPEST simulations demonstrate that turbulent transport plays a similar role to collisional decorrelation of particle orbits and the large turbulent transport leads to Maxwellianization of the particle distribution. We also show the transition of parallel heat flux and flow at the entrance to the divertor plates from the fluid to kinetic regime. For an absorbing divertor plate boundary condition, a non-half-Maxwellian is found due to the substantial collisionality for slow particles.

[1]This work was performed for the U.S. Department of Energy by LLNL under Contract DE-AC52-07NA27344 and by UCSD under Grant No. DE-FG02-04ER54739,

1. Introduction

Modeling of anomalous (turbulence-driven) radial transport in controlled fusion plasmas is necessary for long-time transport simulations. Even in edge plasmas, particle kinetic dynamics becomes important for burning plasma regimes in near future tokamak experiments (such as ITER) because the radial width of the pedestal observed in experiments is comparable to the radial width of individual ion drift orbits, which may lead to a large distortion of the local distribution function from a Maxwellian, and because the ion and electron mean-free-paths are long compared to the connection length for the hot plasma at the top of the edge pedestal (violating the assumptions underlying collisional fluid models). Here the focus is continuum kinetic edge codes such as the transport version of TEMPEST in 4D (radius, poloidal angle, energy, and magnetic moment) [1]. Using anomalous diagonal transport matrix model with velocity-dependent convection and diffusion coefficients allows contact with typical fluid transport models. The goal is to create, effectively, a "kinetic UEDGE [2]" or "kinetic SOLPS [3]" code. Results are presented that combine the anomalous transport model and neoclassical transport owing to ion drift orbits. Comparison is made of the relative magnitudes and possible synergistic effects of the two processes for typical tokamak device parameters.

2. Basic Gyrokinetic Equation with Anomalous Radial Transport

A set of generalized gyrokinetic Vlasov-Poisson equations with anomalous radial diffusion can be written in the gyrocenter coordinate system on an ad hoc basis in the following format.

$$\frac{\partial F_\alpha}{\partial t} \quad + \quad (\bar{\mathbf{v}}_d + \bar{\mathbf{v}}_\parallel) \cdot \frac{\partial F_\alpha}{\partial \bar{\mathbf{x}}_\perp} - Z_\alpha e \left[\left(\frac{B}{B^*} \bar{v}_\parallel + \mathbf{v_{d0}} \right) \cdot \bar{\nabla} \langle \delta\phi \rangle \right] \frac{\partial F_\alpha}{\partial E_0} = C(F_\alpha, F_\alpha)$$

$$- \quad \frac{1}{\mathcal{J}}\frac{\partial}{\partial\psi}\left[\mathcal{J}(RB_p)\Gamma_a\right], \tag{1}$$

$$\bar{\mathbf{v}}_{\mathbf{d}} = \frac{c\mathbf{b}}{Z_\alpha e B^*_\parallel}\times\left(Z_\alpha e\bar{\nabla}\langle\Phi\rangle + \bar{\mu}\bar{\nabla}B\right) + \bar{v}^2_\parallel\frac{M_\alpha c}{Z_\alpha e B^*_\parallel}(\bar{\nabla}\times\mathbf{b}). \tag{2}$$

$$\bar{\mathbf{v}}_{\mathbf{d0}} = \frac{c\mathbf{b}}{Z_\alpha e B^*_\parallel}\times\left(Z_\alpha e\bar{\nabla}\langle\Phi_0\rangle + \bar{\mu}\bar{\nabla}B\right) + \bar{v}^2_\parallel\frac{M_\alpha c}{Z_\alpha e B^*_\parallel}(\bar{\nabla}\times\mathbf{b}). \tag{3}$$

$$\bar{v}_\parallel = \pm\sqrt{\frac{2}{M_\alpha}\left(E_0 - \bar{\mu}B - Z_\alpha e\langle\Phi_0\rangle\right)}, \tag{4}$$

$$B^*_{\parallel\alpha} \equiv B\left[1 + \frac{\mathbf{b}}{\Omega_{c\alpha}}\cdot(v_\parallel\bar{\nabla}\times\mathbf{b})\right], \Omega_{c\alpha} = \frac{Z_\alpha eB}{M_\alpha c}, \mu = \frac{\mathbf{M}_\alpha\mathbf{v}^2_\perp}{\mathbf{2B}}, \tag{5}$$

$$\langle\delta\phi\rangle = \langle\Phi\rangle - \langle\Phi_0\rangle. \tag{6}$$

$$\Gamma_a = U_a F_\alpha - D_a(RB_p)\frac{\partial F_\alpha}{\partial\psi}. \tag{7}$$

Here $Z_\alpha e$, M_α are the electric charge and mass of electrons ($\alpha = e$), ions ($\alpha = i$), μ is the guiding center magnetic moment, Φ_0 is the prescribed electric potential, and $\delta\phi$ can be solved from the gyrokinetic Poisson equation [4, 5]. The left-hand side of Eq. (1) describes particle motion in electric and magnetic fields. C_α is the Coulomb collision operator. The over-bar is used for the gyrocenter variables and $\langle\ \rangle$ denotes gyro-angle averaging. A radial convection of anomalous particle flux Γ_a in 5D phase space is added to mock up the effect of turbulent transport. Turbulent transport is modeled as a combination of advection and diffusion, as is conventionally done in fluid descriptions. Here $U_a(\psi)$ is the advection velocity, and D_a is the diffusion coefficient, which generally depend on position (ψ) and velocity (E_0, μ). Specifying different velocity dependences allow a separate control of diffusion for particles D, heat χ and momentum χ_φ. Adding an independent advection velocity U_a also allows $D_a(\psi, E_0, \mu)$ to be positive for all velocities and provides flexibility, speed (compared to coupling turbulence), and comparison to fluid models. Taking for the diffusion coefficient a quadratic polynomial in energy E_0, one can obtain moment equations which in the collisional (Maxwellian) limit reproduce fluid transport equations with an arbitrary combination of diagonal particle and thermal transport coefficients (a 5-variables

transport model). The detailed coefficient form will be given in a future publication [6].

In the rest of the paper, we will present simulations for a single ion species and no electric field ($\Phi = \Phi_0 = \delta\phi = 0$).

3. TEMPEST Simulation Results of Plasmas Transport in Circular Geometry

Using the freedom to specify velocity dependence, and with the incorporation of an advection term, it is possible to reproduce the effect of an arbitrary diagonal transport matrix in fluid equations when the kinetic code's distribution function is Maxwellian. The advection is required to maintain global positivity of the kinetic code's diffusion coefficient. This model has been combined with a density and energy-conserving Krook collision model and verified, in circular core geometry, with test cases. For the diffusion coefficient with a simple linear dependence over energy E_0, advection velocity $U_a(\psi)$ and diffusion coefficient D_a can be written in the following form (2-variables model):

$$U_a = D_n \left[(RB_p) \frac{\partial \ln T_\alpha}{\partial \psi} \right], \tag{8}$$

$$D_a = \frac{4}{5} \left(2D_n - \frac{1}{3}\chi_n \right) \frac{v^2}{v_{Ti}^2}. \tag{9}$$

Here the diffusivity D_n and thermal conductivity χ_n are two separate input parameters for the model. For a Maxwellian distribution function, the 2-variables model can be further reduced to a 1-variables model and the corresponding analytical moment fluxes can be written as

$$\chi_n = \frac{7}{2} D_n, \tag{10}$$

$$D_a = \frac{2}{3} D_n \frac{v^2}{v_{Ti}^2}, \tag{11}$$

$$\Gamma_n = -D_n \left[(RB_p) \frac{\partial n}{\partial \psi} \right], \tag{12}$$

$$Q_n = -\frac{5}{2} D_n T \left[(RB_p) \frac{\partial n}{\partial \psi} \right] - \chi_n \left[n (RB_p) \frac{\partial T_\alpha}{\partial \psi} \right]. \tag{13}$$

Therefore in a typical fluid case with a Maxwellian distribution function, the thermal

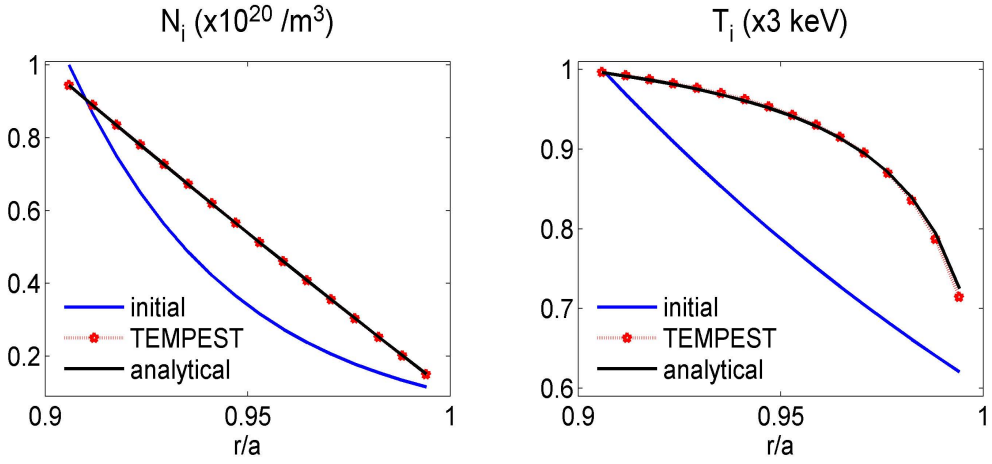

FIG. 1: Poloidally- averaged initial and final steady-state ion density and temperature profiles in a circular geometry. For a 2-variables diffusion-advection model in Eqs. (8) and (9), the diffusivity $D_n = 10m^2/s$ and thermal conductivity $\chi_n = 35m^2/s$.

conductivity χ_n is no longer an independent control. As a test case, we conduct a TEMPEST diffusion simulation in a Ring geometry without drifts and collision. The Dirichlet boundary conditions at the radial boundaries are used with $N_{io} = 0.1N_{ix}$ and $T_{io} = 0.6T_{ix}$, where N_{ix} and T_{ix} are the density and temperature at the inner most radial boundary surface, and N_{io} and T_{io} are the density and temperature at the outer most radial boundary surface. The initial condition is an exponential variation over the radial position. Figure 1 shows poloidally-averaged initial and final steady-state ion density and temperature profiles. For a 2-variables diffusion-advection model in Eqs. (8) and (9), the diffusivity $D_n = 10m^2/s$ and thermal conductivity $\chi_n = 35m^2/s$, where the fluid relationship between D_n and χ_n in Eqs. (10) is used by guidance to choose their relative values. The

steady-state solution is one for divergence of fluxes being equal to zero. As shown, both density and temperature variation agree with analytical expectation.

4. TEMPEST Simulation Results of Plasmas Flows and Heat Fluxes in Divertor Geometry

In this section, a simplified version of the diffusion model is used, where $U_a = 0$ and $D_a = D = const.$ TEMPEST simulations were carried out for plasma transport and flow dynamics in a single-null tokamak geometry, including the pedestal region that can extend across the separatrix into the scrape-off layer (SOL) and private flux region. The core radial boundary particle distribution is a fixed Maxwellian $F_{M\alpha}$ with $N_{0\alpha}$, $T_{0\alpha}$ and $U_{\|0\alpha}$, the exterior radial boundary particle distribution is a Neumann boundary condition with $\partial F_\alpha(\psi, \theta, E, \mu)/\partial\psi|_w = 0$ and an absorbing divertor plate boundary condition during a simulation, where α represents the particle species. The initial ion density and temperature profiles $n_i(\psi) = N_{ix}\exp(-\ln(N_{ix}/N_{io})\psi/L_\psi)$, and $T_i(\psi) = T_{ix}\exp(-\ln(T_{ix}/T_{io})\psi/L_\psi)$ with $T_{ix} = 300eV, T_{io} = 0.1T_{ix}, N_{ix} = 1\times10^{19}m^{-3}$, and $N_{io} = 0.1N_{ix}$, Here an energy dependent Lorentz collision operator is used with the local density and temperature calculated from the corresponding moment of the instantaneous distribution function. Given boundary conditions and initial profiles, the interior plasma in the simulations should evolve into a steady state. The mesh resolutions are $n_\psi = 40, n_\theta = 80, n_E = 25$, and $n_\mu = 30$. A non-uniform μ-mesh is used. In the simulations Φ is set to zero and there is no recycling for simplicity.

4.1 Simulation Results for D=0.1m^2/s

In this section, we present the transport simulation results with a given anomalous diffusion coefficient D=0.1m^2/s. Fig. 2(a) shows the contour plot of steady-state ion temperature profile. The time history of ion temperature at various poloidal positions is shown in Fig. 2(b), indicating that a steady-state solution is achieved. The radial profiles of ion temperature are shown in Fig. 2(c) for outside midplane (black), inner divertor plate (blue) and outer divertor plate (red); initial profiles are in dashed line. The ion temperature at the divertor plates peaks near the separatrix in the SOL due to the dominant parallel streaming. Because of the parallel endloss [in addition to radial transport (neoclassical plus anomalous)] in the SOL, ion midplane temperature slope becomes steeper across the separatrix. It is worth pointing out the convention of the horizontal axis used throughout this paper when plotting the midplane radial profiles together with radial profiles at the divertor plates. The poloidal position of labeled divertor plates is the first (for inner divertor plate) and the last (for outer divertor plate) interior poloidal nodal point, one poloidal cell away from the position where the divertor boundary conditions have been actually set at any radial location. The data in the SOL at the divertor plates (curves on the right side of the separatrix) are projected to the outer midplane and are plotted as a function of the normalized distance across the separatrix; The data in the private flux region (curves on the left side of the separatrix at the divertor plates) are projected to the outer midplane and are plotted as a function of the normalized distance across the separatrix, however, which should be interpreted as a function of radial index.

Fig. 3(a) shows the contour plot of steady-state ion parallel heat flux for the anomalous diffusion coefficient D=0.1m^2/s. The radial profiles of ion parallel velocity $U_{\|i}$ and parallel

heat flux $Q_{\|i}$ are shown in Fig. 3(b) and Fig. 3(c) for outside midplane (black), inner midplane (lime green), inner divertor plate (blue) and outer divertor plate (red). The benchmarking solution (in magenta) at the outer divertor plate is obtained by (1) dropping all terms except parallel streaming in Eq. (1); (2) in steady-state, $\partial F_\alpha/\partial t = 0$; (3) taking the 0^{th} and 1^{st} moment of parallel velocity and integrating along the field line between X-point and divertor plate. As shown, both ion parallel flow and parallel heat flux agree with benchmarking solution, indicating that parallel streaming is the dominant particle dynamics in the divertor leg regions below X-point. Ion parallel flow peaks close to the separatrix at various poloidal locations in the SOL due to the dominant parallel streaming; in contrast, the midplane heat flux peaks away from the separatrix in the SOL, indicating the finite ion orbit effect as the heat flux is higher moment of the ion distribution function than the parallel flow.

4.2 Anomalous Diffusion Scan

A series of TEMPEST simulations is conducted to investigate the transition of midplane pedestal parallel heat flux and flow from the neoclassical to turbulent limit and the transition of divertor parallel heat flux and flow from the kinetic to the fluid regime via an anomalous transport scan. In Fig. 4, we show scans of ion parallel flow $U_{\|i}$ and ion parallel heat flux $Q_{\|i}$ via anomalous diffusion coefficient D calculated by TEMPEST for the DIII-D geometry. Each data point of ion parallel flow $U_{\|i}$ and ion parallel heat flux $Q_{\|i}$ is obtained from the peak midplane value and peak outer divertor plate value for each simulation with the corresponding anomalous diffusion coefficient D. The mid-plane plasma exhibits neoclassical behavior: the ion parallel heat flux decreases as D increases since the large D flattens the plasma profiles, leading to smaller parallel flux as neoclassical theory

predicts. In contrast, at the divertor plate, endloss and collision dominates the dynamics. The ion parallel heat flux decreases as D decreases. The theoretical expectation is a half-Maxwellian ion distribution at the divertor entrance due to the absorbing divertor plate boundary condition. If so, the calculated ion parallel flow should be $U_{\|i} = 0.28 v_{Ti}$, as marked green star on Fig. 4 (a), while TEMPEST simulation yields a value $U_{\|i} = 0.03 v_{Ti}$; the calculated ion parallel heat flux should be $Q_{\|i} = 0.56 P_i v_{Ti}$, as marked purple star on Fig. 4 (b), while TEMPEST simulation yields a value $Q_{\|i} = 0.15 P_i v_{Ti}$. TEMPEST simulations yield an ion parallel flow and heat flux mush smaller than that calculated from the half-Maxwellian due to the substantial collisionality for slow particles. As a reminder of our convention, the poloidal position of labeled divertor plates is the first (for inner divertor plate) and the last (for outer divertor plate) interior poloidal nodal point, one poloidal cell away from the position where the divertor boundary conditions have been actually set at any radial location. However, the distribution function right at the divertor plate (at the corresponding ghost nodal point) obeys absorbing boundary conditions as been applied and the flux is that from a half-Maxwellian.

Ion distribution functions are shown in Fig. 5 at various poloidal positions as indicated within close proximity to the separatrix in the SOL for anomalous diffusion coefficient D=$1 m^2/s$. The contours of parallel heat flux $Q_\|(R, Z)$ is shown in the center with four companion plots for normalized ion distribution function vs parallel velocity $v_\|$. In each companion plot, four curves represent different μ-class, the guiding magnetic moment. Here $\mu_n = n\Delta\mu$, n=0,1,2,3,4, and $\Delta\mu$ is the μ-spacing. The dotted line F_m represents Maxwellian distribution function. As shown, the distribution is not Maxwellian at mid-plane and is not half-Maxwellian at the divertor plates either, which is responsible for the reduced parallel flow and heat flux at the divertor plates as shown in Fig. 4. The

scan of midplane ion distribution function (normalized) vs anomalous diffusion coefficient D is shown in Fig. 6. As D increases, the distribution function approaches Maxwellian distribution, which demonstrate that turbulent transport plays a similar role to collisional decorrelation of particle orbits and the large turbulent transport leads to Maxwellianization of the particle distribution.

To further corroborate the observation, we calculate two characteristic times: particle banana orbit time $\tau_b = qR/(\sqrt{\epsilon} v_{Ti})$ and diffusion time $\tau_D = L_P^2/D$. Here q is the safety factor, R the major radius, ϵ the inverse aspect ratio, v_{Ti} ion thermal speed, $L_P = |\nabla(\ln P)|^{-1}$ the pressure gradient scale length calculated from the steady-state pressure profile. For given parameters, $\tau_b \simeq 100\mu s$, the corresponding ratio of diffusion time to particle banana orbit time is calculated in the following: $\tau_D/\tau_b = 10$ for D=0.1m^2/s, $\tau_D/\tau_b = 1$ for D=1m^2/s, and $\tau_D/\tau_b = 0.1$ for D=10m^2/s. To mimic the classification of neoclassical regimes, the ratio τ_D/τ_b defines the effective banana regime for for D=0.1m^2/s, the effective plateau regime for for D=1m^2/s, and the effective collisional regime for for D=10m^2/s.

4.3 Initial Ion Density Scan

A series of TEMPEST simulations is also conducted to investigate the transition of midplane pedestal parallel heat flux and flow from the neoclassical to turbulent limit and the transition of divertor parallel heat flux and flow from the kinetic to the fluid regime via initial ion density scan for $N_{ix} = (1 \times 10^{19}, 1 \times 10^{20}, 1 \times 10^{21}) m^{-3}$ with $T_{ix} = 300eV, T_{io} = 0.1T_{ix}$, $N_{io} = 0.1N_{ix}$ and D=0.1m^2/s. As density increases, the collisionality increases, which leads to an increased neoclassical diffusion. Ion parallel flow and heat flux follow a similar trend as seen in the previous section: the midplane ion parallel

heat flux and flow decreases as density increases; in contrast, divertor ion parallel heat flux and flow increases as density increases.

5. Summary

We report on the development and application of 4D version of TEMPEST with anomalous radial transport added, a fully nonlinear (full-f) gyrokinetic code, to edge transport simulations. The formulation and implementation of a velocity-dependent diffusion/advection operator to mock up the effect of anomalous transport in 4D (radius, poloidal angle, energy and magnetic moment) TEMPEST has been presented. Transport coefficients can be assigned so as to be equivalent in the highly collisional limit to fluid models for comparisons. A test simulation is done using the model, yielding varying density and temperature profiles in ring geometry which compare well with the analytical expectations. Using a simplified version of this diffusion model (constant-in-velocity diffusion coefficient only), we are able to obtain steady solutions of neoclassical transport together with model anomalous transport in divertor geometry. A series of TEMPEST simulations were conducted to investigate the transition of midplane pedestal heat flux and flow from the neoclassical to turbulent limit and the transition of divertor heat flux and flow from the kinetic to the fluid regime via a density-scan and an anomalous transport scan. The TEMPEST simulations demonstrate that turbulent transport plays a similar role to collisional decorrelation of particle orbits and the large turbulent transport leads to Maxwellianization of the particle distribution. The mid-plane plasma exhibits neoclassical behavior: the ion parallel heat flux decreases as D increases since the large D flattens the plasma profiles, leading to smaller parallel flux as neoclassical theory predicts. In contrast, at the divertor plate, endloss and collisions dominate the dynamics. The ion parallel heat

flux decreases as D decreases. The theoretical prediction is a half-Maxwellian ion distribution at the divertor entrance, however, TEMPEST simulations yield an ion parallel heat flux smaller than that calculated from the half-Maxwellian due to the substantial collisionality for slow particles and exotic particle orbit effects.

Acknowledgments

We thank Drs. J. Candy, B. I. Cohen, P. Colella, A. M. Dimits, M. R. Dorr, J. A. Hittinger, G. D. Kerbel, D .D. Ryutov, P. B. Snyder, M. V. Umansky, and Z. Xiong for fruitful physics discussions.

References

[1] X. Q. Xu, Z. Xiong, M. R. Dorr, J. A. Hittinger, *et al.*, *Nucl. Fusion* **47**, 809 (2007).

[2] T. D. Rognlien, B. J. Braams, and D. A. Knoll, Contrib.Plasma Phys. **36**, 105(1996); T. D. Rognlien, D. D. Ryutov, N. Mattor, and G. D. Porter, Phys. Plasmas **6**, 1851 (1999).

[3] D. P. Coster, X. Bonnin, G. Corrigan, *et al.*, Phys. Scr. **T108**, 7-13(2004).

[4] X. Q. Xu, *Phys. Rev. E.* **78**, 016406 (2008).

[5] X. Q. Xu, E. Belli, K. Bodi, *et al.*, NUCLEAR FUSION, **49**, 065023 (2009).

[6] K. Bodi, *Anomalous radial transport in tokamak edge plasma*, PhD thesis, University of California, San Diego, USA, 2009.

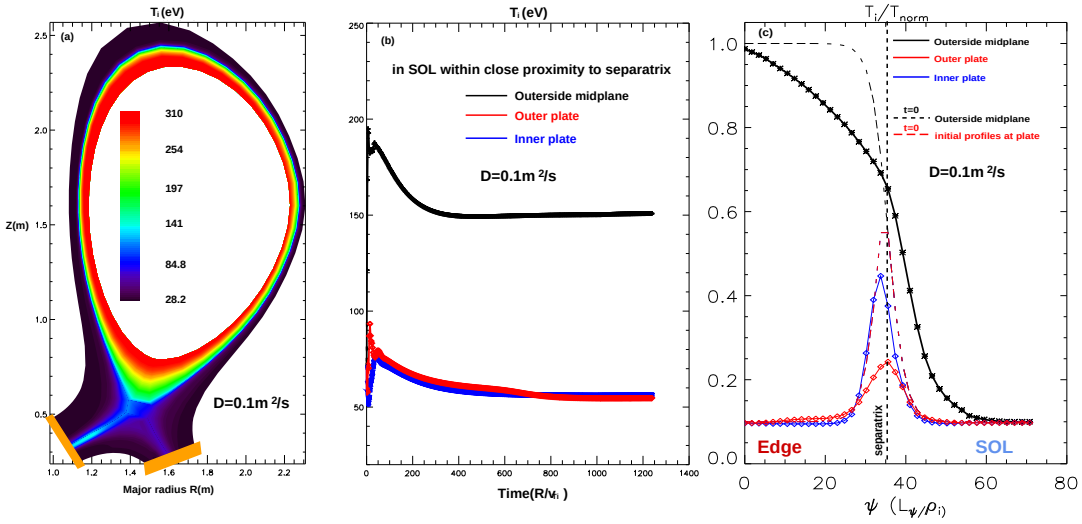

FIG. 2: (a) The contours of ion temperature $T_i(R, Z)$ in the divertor geometry D=0.1m^2/s. (b) A time history of ion temperature at various poloidal positions: outside midplane (black), inner divertor plate (blue) and outer divertor plate (red). (c) The radial profiles of ion temperature T_i at initial t=0 and final steady-state, and at various poloidal positions: outside midplane (black), inner divertor plate (blue) and outer divertor plate (red). The data in the SOL at the divertor plates are projected to the outer midplane and are plotted as a function of the normalized distance across the separatrix; The data in the private flux region (curves on the left side of the separatrix at the divertor plates) are projected to the outer midplane and are plotted as a function of the normalized distance across the separatrix, however, should be interpreted as a function of radial index.

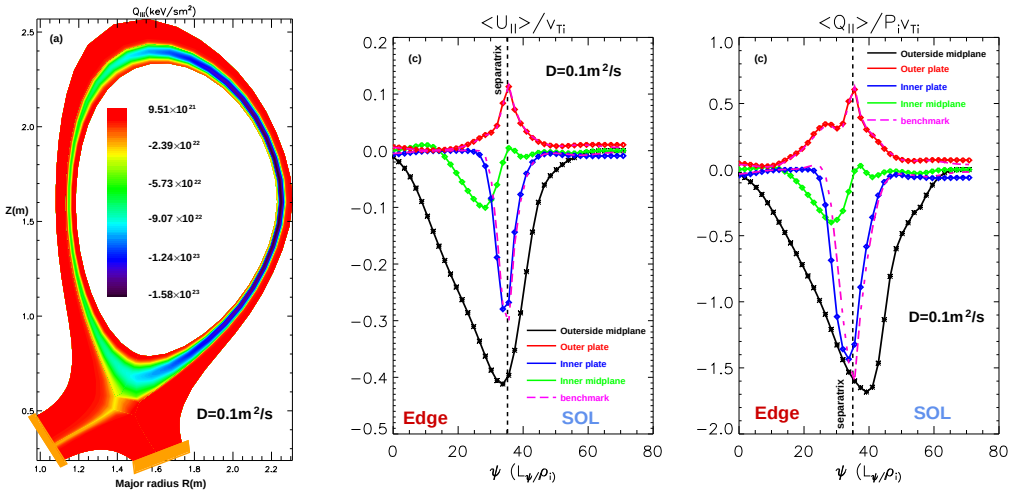

FIG. 3: (a) The contours of parallel heat flux $Q_{\|}(R,Z)$ in the divertor geometry for D=0.1m^2/s. (b) The radial profiles of parallel velocity $U_{\|i}$ at various poloidal positions: outside midplane (black), inner midplane (lime green), inner divertor plate (blue), outer divertor plate (red), and a benchmarking solution (in magenta) at the outer divertor plate. (c) The radial profiles of parallel heat flux $Q_{\|i}$ at various poloidal positions: outside midplane (black), inner midplane (lime green), inner divertor plate (blue) and outer divertor plate (red), and a benchmarking solution (in magenta) at the outer divertor plate. In Fig. 3 (b) and (c), the data in the SOL at the divertor plates are projected to the outer midplane and are plotted as a function of the normalized distance across the separatrix; The data in the private flux region (curves on the left side of the separatrix at the divertor plates) are projected to the outer midplane and are plotted as a function of the normalized distance across the separatrix, however, should be interpreted as a function of radial index.

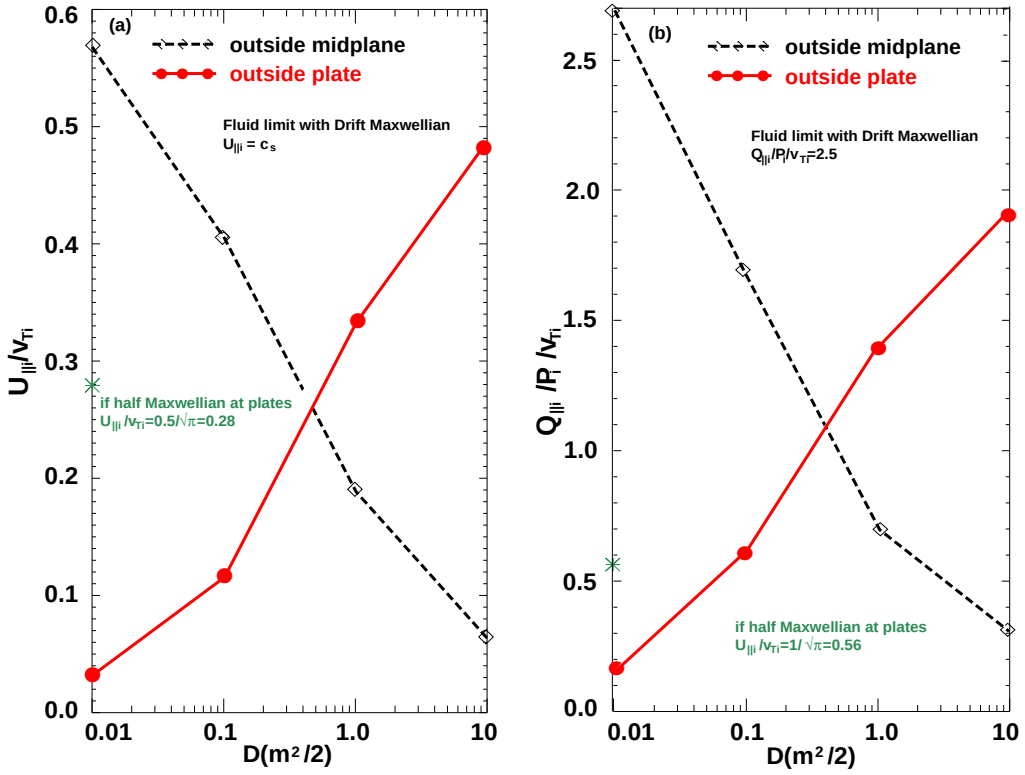

FIG. 4: (a) A scan of ion parallel velocity via anomalous diffusion coefficient D calculated by TEMPEST for the DIII-D geometry. (b) A scan of ion parallel heat flux via anomalous diffusion coefficient D calculated by TEMPEST for the DIII-D geometry.

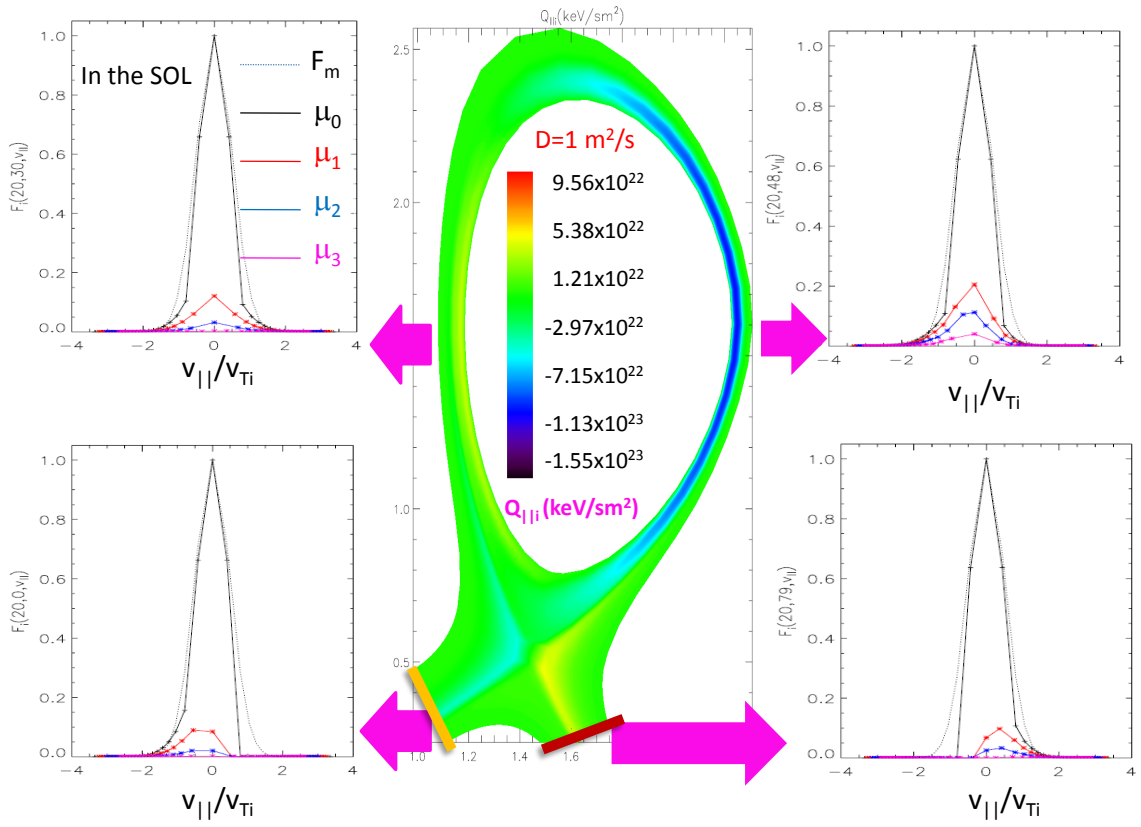

FIG. 5: A contour of ion parallel heat flux in radial-poloidal plane for $D = 1m^2/s$ and ion distribution function (normalized) at various poloidal locations calculated by TEMPEST for the DIII-D geometry. Here $\mu_n = n\Delta\mu$, n=0,1,2,3,4, and $\Delta\mu$ is the magnetic moment μ-spacing.

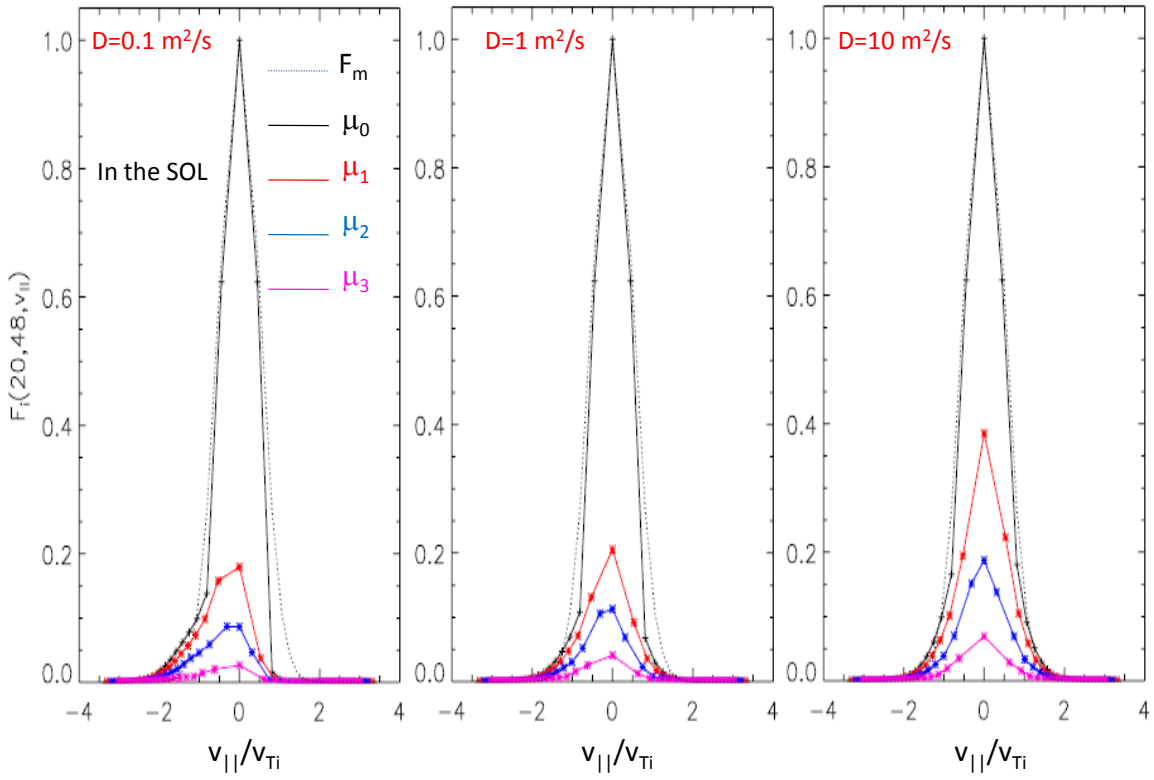

FIG. 6: A scan of ion distribution function (normalized) at midplane via anomalous diffusion coefficient D calculated by TEMPEST for the DIII-D geometry. Here $\mu_n = n\Delta\mu$, n=0,1,2,3,4, and $\Delta\mu$ is the magnetic moment μ-spacing.